Applied Catalysis B: Environmental 217 (2017) 144–153

Contents lists available at ScienceDirect

Applied Catalysis B: Environmental

journal homepage: www.elsevier.com/locate/apcatb

Research Paper

Trapped metallic cobalt nanoparticles in doped porous graphite: An electrocatalyst that gets better over reaction time

Guilherme M. Pereira, Thelma S.P. Cellet, Ricardo H. Gonçalves, Adley F. Rubira, Rafael Silva*

Departamento de Química, Universidade Estadual de Maringá (UEM) - Av. Colombo 5790 - CEP 87020-900, Maringá, Paraná, Brazil

ARTICLE INFO

Article history:
Received 2 January 2017
Received in revised form 26 April 2017
Accepted 19 May 2017
Available online 20 May 2017

Keywords:
Self-activation
Graphitic porous carbon
Metallic cobalt nanoparticles
Melamine-formaldehyde resin
Water oxidation reaction

ABSTRACT

Hybrid materials synthesis is a pathway to integrating unstable inorganic phases in a protective matrix, as an approach to phase stabilization in harsh environments and to use the unique catalytic properties of such metastable phases. Here, we show a polymer precursor method to synthesize nitrogen-doped carbon nanomaterials from melamine-formaldehyde resin with Co^{2+} ions coordinated in the precursor material. Co^{2+} ions are reduced during the pyrolysis process to form metallic nanoparticles. Nitrogen-doped carbon nanotubes, with high nitrogen content, are obtained at pyrolysis temperature of 800 °C or 900 °C. When lower temperature is used (i.e. 700 °C), porous amorphous carbon is obtained. At the highest temperature used (1000 °C), carbon matrix with low nitrogen content is produced, having porous graphitic carbon structure. Graphitic carbon structure and metallic cobalt showed impressive catalytic activity toward water electrooxidation reaction, similar to benchmark catalysts for OER. The stability studies of the electrocatalyst showed an extraordinary 52% current density improvement in the first 8 h of OER, and then a very stable pattern is verified. After 12 h of applied potential, Tafel slope decreases to 57 mV dec^{-1}, which is characteristic of very fast surface kinetics, and therefore it is a promising material to become a reliable alternative to anode manufacture for OER.

1. Introduction

Carbon materials have consistently been in the forefront of the development of nanoscience and nanotechnology [1–3]. Structure–properties correlations are univocal for carbon materials and each carbon nanomaterial has at least a unique attribute that stands out [4–6]. Therefore, different structural shapes are known, e.g. nanospheres, nanotubes, nanosheets and nanoneedles [7–11]. However, the most recent groundbreaking outcome on carbon materials is not due to the carbon nanomaterial shape, but to the chemical composition of carbon-based materials [12–14]. In fact, the introduction of heteroatoms, mainly nitrogen, to carbonaceous structures has added intrinsic catalytic activities toward several electrochemical processes to the long list of special features exhibited by carbon-based materials [15–17].

Intrinsically active carbon materials have shifted the paradigms about the catalysis of electrons transfer reactions and establish new directions on the development of renewable energy technologies, due to advances on oxygen reduction reaction (ORR), and both water splitting semi-reactions, hydrogen and oxygen evolution reactions, HER and OER, respectively [11,18]. However, with the accession of doped-carbon materials new challenges appears mainly referent to the improvement of their stability and conductivity [19]. Most of the doped-carbon materials with outstanding catalytic activity reported is highly porous carbon with amorphous structure [20,21]. Materials with elevated porosity have the advantage of raised surface area, however the conductivity is normally low due to the amorphous structure, and therefore the existence of large content of defects on the carbon basal plane [22]. One possible approach to high surface area and organized materials is the synthesis of structured carbon materials, which have lower electrical resistance and higher chemical stability than amorphous carbon, such as heteroatom-doped graphene or carbon nanotubes (CNT) [23–26].

Both graphene and CNT demonstrated in numerous reports their importance for electrocatalysts preparation and as constituent material for electrode in charge storage devices [27,28]. Therefore, simplified synthetic methods that can be carried out to produce large amounts of high quality structured doped-carbon materials will be a step forward in electrocatalysis with noble-metal free cat-

* Corresponding author.
E-mail address: rsilva2@uem.br (R. Silva).

http://dx.doi.org/10.1016/j.apcatb.2017.05.056
0926-3373/

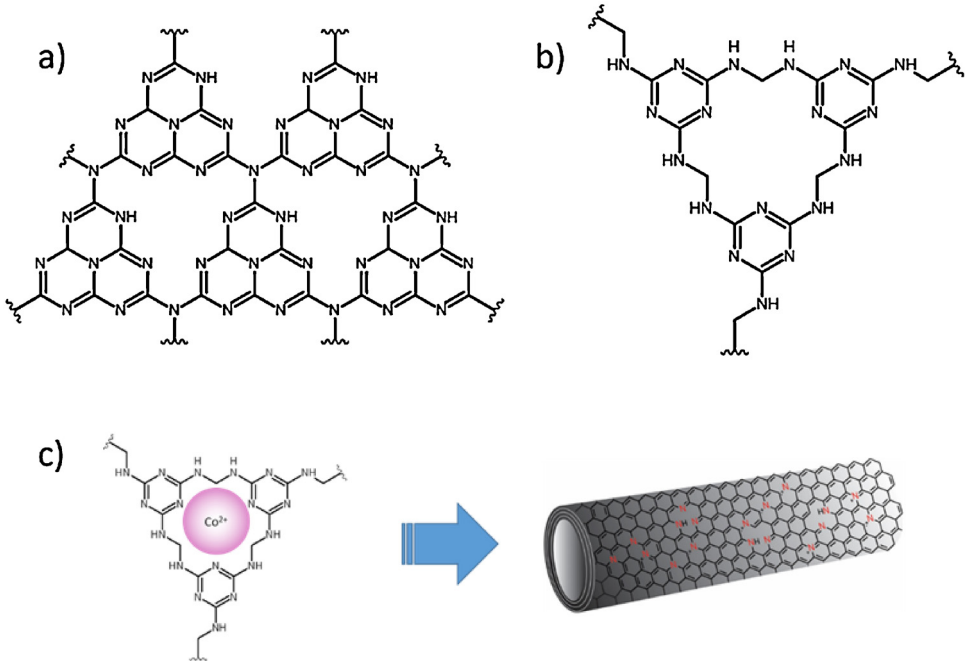

Scheme 1. Chemical structure of graphitic carbon nitrate (g-C_3N_4) (a), melamine-formaldehyde resin (b), and the scheme representing the use of cobalt doped MFR to prepare N-CNT (c).

alysts. In the case of N-doped CNT (N-CNT), their synthesis can be accomplished by chemical vapor deposition (CVD) or by the carbonization of graphitic carbon nitrides (g-C_3N_4) containing metal ions [29,30]. The method based on the pyrolysis of a molecular precursor has advantages over CVD methodology in relation to process scaling up. Large amount of N-CNT can be easily prepared by simple carbonization of metal-doped graphitic carbon nitride [30]. However, graphitic carbon nitride synthesis is a bottleneck for scaling up. Melamine-formaldehyde resin (MFR) is a feasible alternative to N-CNT, since the chemical structure of MFR is compared to graphitic carbon nitride (Scheme 1a and b). Moreover, MFR has chemical structure with high N to C ratio and melamine rings cross-linked in a tridimensional high molar weight structure. MFR is easily found in daily routine products, for instance as melamine foams (i.e. magic eraser) and plastic laminate (Formica®). Additionally, MFR differs from other thermoset polymers due to their capability to form soft and mechanically strong foams, which is associated with special features such as very high thermal stability and fire retardant ability. The production of MFR is a very simple chemical process. It consists on the polymerization of melamine with formaldehyde, which can be catalyzed by a strong base or acid. It is worth to note that melamine is an abundant feedstock, since it can be produced by the thermal decomposition of urea [31].

In addition, the use of MFR as precursor to the preparation of N-doped carbon nanomaterials is a straightforward approach to integrate metal phases in the final carbon matrix. In fact, the metal is fundamental to the graphitization process, and it can lead to special structures, such as N-doped carbon nanotubes. The catalytic properties of transition metal phases can be boosted for electrochemical processes when the metal phases are integrated to a highly conductive, stable, and intrinsically active carbon matrix [32]. A number of cobalt phases have already proved to be efficient for water oxidation reaction [33,34]. In same special cases, cobalt oxide phases provide outstanding overpotential (η), as good as 300 mV at current density of 10 mA cm^{-2}, which is very competitive when compared to well-known and efficient IrO_2 and RuO_2 catalysts [35,36]. Recently, Wu et al. reported the preparation of Co nanoparticles (CoNPs) by the thermal decomposition of cobalt carbonyl [$Co_2(CO)_8$] in 1,2,3,4-tetrahydronaphthalene solution with oleic acid and dioctylamine as surfactants. The obtained CoNPs are protected by carbon, and the carbon protective layer works to prevent the oxidation of the Co metallic phase. An overpotential of 400 mV was observed when CoNPs capped by carbon are applied for OER.

In the present work, N-doped carbon materials with metallic cobalt phase embodied are prepared from thermal decomposition of MFR doped with trace amount of cobalt ions. MFR@Co pyrolysis are carried out at different temperatures to obtain different N-doped carbon structures, amorphous porous carbon, CNT, and graphitic porous carbon. The cobalt is reduced from its initial 2+ oxidation state to form metallic CoNPs. In addition, the prepared samples were tested as catalysts toward oxygen evolution reaction in strong basic condition.

2. Experimental

2.1. Materials

$Co(NO_3)_2$, formaldehyde solution (37%), Poly(ethylene glycol)-block-poly(propylene glycol)-block-poly(ethylene glycol) ((PEG)20(PPG)70(PEG)20) (Pluronic® 123), average molecular weight ~5800 Da) and isopropanol were obtained from Sigma-Aldrich (Brazil). NaOH, KOH were purchase from Synth (Brazil). Melamine commercial was donated by GPC Quimica S.A (Brazil).

2.2. Synthesis of melamine-formaldehyde resin (MFR)

P123 (2.5 g) was dissolved in distilled water (150 mL) at 60 °C. After complete P123 dissolution, melamine (2.2 g, 17.6 mmol) was added. The mixture was kept under stirring for 3 h, then formaldehyde (1.6 g, 53.0 mmol) was added to the mixture followed by 3.8 mmol of NaOH. The mixture was kept under stirring for 5 h. Cobalt doping was carried out prior the thermal treatment step by the addition of $Co(NO_3)_2$. Cobalt (II) nitrate was added at molar ratio of 1:16 in relation to melamine. A blank sample was also prepared without the addition of cobalt. After the addition of cobalt nitrate,

the mixture was stirred by an additional 30 min. To complete the synthesis, the mixture was transferred to an oven at 180 °C for 4 h to promote polymer crosslinking.

2.3. Resins pyrolysis

Carbonization process was carried out in a tubular oven under nitrogen atmosphere with a continuous N_2 flow of 20 mL min^{-1}. A temperature program with different stages was used. Once the sample was placed in the oven, the temperature was increased from the initial room temperature up to 200 °C with heating ramp of 1 °C min^{-1} and the temperature was kept at 200 °C for 30 min. The temperature was increased to 300 °C at 1 °C min^{-1} and kept at 300 °C for 30 min. Then, the temperature was increased to the final heating temperature with heating ramp of 3 °C min^{-1}. Samples were prepared with different final temperatures (700 °C, 800 °C, 900 °C and 1000 °C). The samples were kept at the final temperature for 30 min. Then, the system was cooled down to room temperature and the sample was removed and washed in water to remove NaOH used in the polymerization step. Therefore, the solid was copiously washed to neutral pH and the solid was placed in an oven at 60 °C for 12 h to dry.

2.4. Characterization

Textural features of the samples were obtained from N_2 adsorption and desorption experiments. The measurements were carried out at 77 K using a QuantaChrome Nova 1200. Samples were degassed for 12 h at 150 °C at 10 μmHg. Surface areas were calculated using Brunauer–Emmett–Teller (BET) method and the pore distributions were evaluated using BJH method. Cobalt phases and carbon matrix crystallinity were determined by X-ray diffraction (XRD), performed in a Shimadzu Lab-X XRD6000, using an X-ray incident beam with wavelength of 0.154 nm and the 2θ scattered angle observed from 10 to 60°. Raman spectra were performed with solid samples using a laser of wave length of 532 nm and 5 mW of power on a Bruker Senterra micro-Raman spectrometer. The thermal stability and the amount of Cobalt in each sample was determined by thermogravimetric analysis (TGA) using a TGA-Q50 from TA Instruments under flow of air of 100 mL min^{-1} and 10 °C min^{-1} of heating rate. X-ray photoelectron spectroscopy (XPS) was carried out in a Thermo Scientific K-alpha spectrometer using an Al K-α as monochromatic X-ray source. The morphology of the samples were verified by transmission electron microscopy (TEM) and scanning electron microscopy (SEM). TEM images were collected in a JEOL 1400, operating with acceleration voltage of 120 KV. SEM images were obtained in a Shimadzu Supercan 550S, using acceleration voltage 15 kV and secondary electrons detector.

Electrocatalytic activity was tested by linear sweep voltammetry (LSV) performed in an AutoLab model pgstat302N. Glassy carbon electrode was used as the working electrode, graphite rods used as counter electrode and saturated calomel electrode as reference electrode. The measurements were carried out using a N_2 saturated solution of KOH 1.0 mol/L as electrolyte. The samples were tested by supporting the powdered materials in the surface of glassy carbon electrode. A catalyst ink was prepared to stick the powdered materials to the polished surface of the electrode. Catalysts inks were prepared by dispersing a determined amount of samples in 1.5 mL of a 1:3 isopropanol to water mixture. 165 μL of 5% nafion solution were added as binder to the ink mixture. Then, the inks were dropped to the surface of the glassy carbon electrode. The volume of ink added to the glassy carbon electrode is used to control the amount of catalyst deposited in the glassy carbon electrode. For all measurements the loading of the catalyst on the surface were kept at 0.1 mg cm^{-2}. Linear Sweep Voltammetry (LSV) was recorded at scan rate of 20 mV s^{-1} and at 1000 rpm. Current density is normalized in function of the electrode geometric surface area, unless otherwise specified.

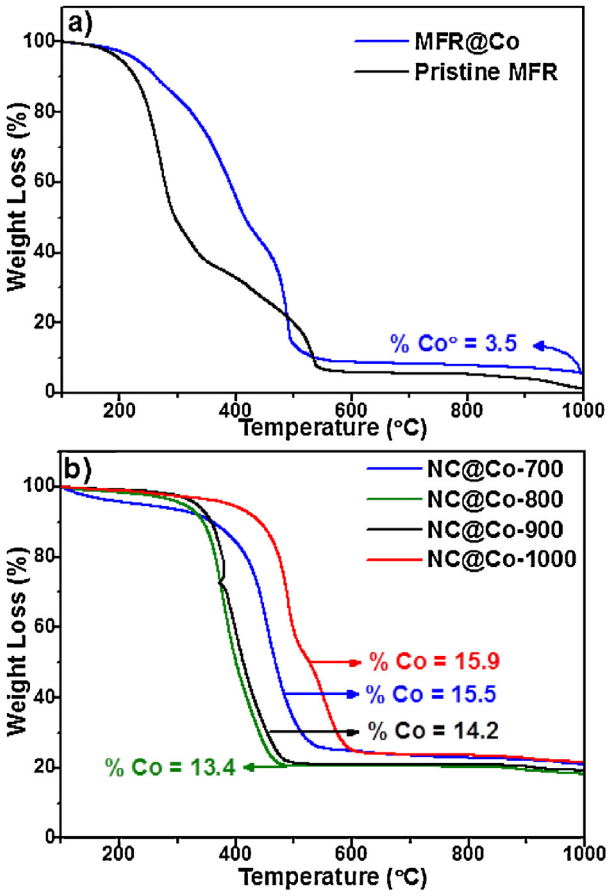

Fig. 1. Thermogravimetric curves of the (a) precursor materials and (b) final hybrid materials in synthetic air.

3. Results and discussion

Melamine-formaldehyde resin is prepared through basic catalyzed polymerization and the Co^{2+} are incorporated in the resin during the polymerization step to provide an uniform distribution of the Co^{2+} ions. The general properties of the resin, such as thermal stability and stiffness are governed by the degree of cross-links in the polymeric matrix that can be controlled by the melamine to formaldehyde ratio. Therefore, a 1:3 molar ratio of melamine to formaldehyde was used to achieve the highest thermal stability based on the result reported by Anderson et al., who found that 1:3 ratio of melamine to formaldehyde is able to produce a MFR with onset degradation temperature at ca. 375 °C [37]. The thermal stability of the carbon precursor affects the overall quality of the carbon material.[38] The degradation of the C-C bond at low temperature reduces the production of low molecular weight species that are volatilized in the thermal treatment step. Therefore, the sample were slowly heated at 1 °C min^{-1} with two intermediate heating stages of 30 min at 200 °C and at 300 °C before the temperature be increased to the final carbonization temperature.

Thermogravimetric curves of the pure MFR and MFR@Co in synthetic air are shown in Fig. 1a. MFR undergoes a fast degradation process in the region from 200 °C to 300 °C, which leads to weight loss near to 70%. This first degradation step is affected by the presence of Co^{2+} in the resin. In the TGA curves of MFR@Co can be observed that the addition of Co^{2+} retards the weight loss process by shift the weight loss to higher temperature. It indicates that Co^{2+}

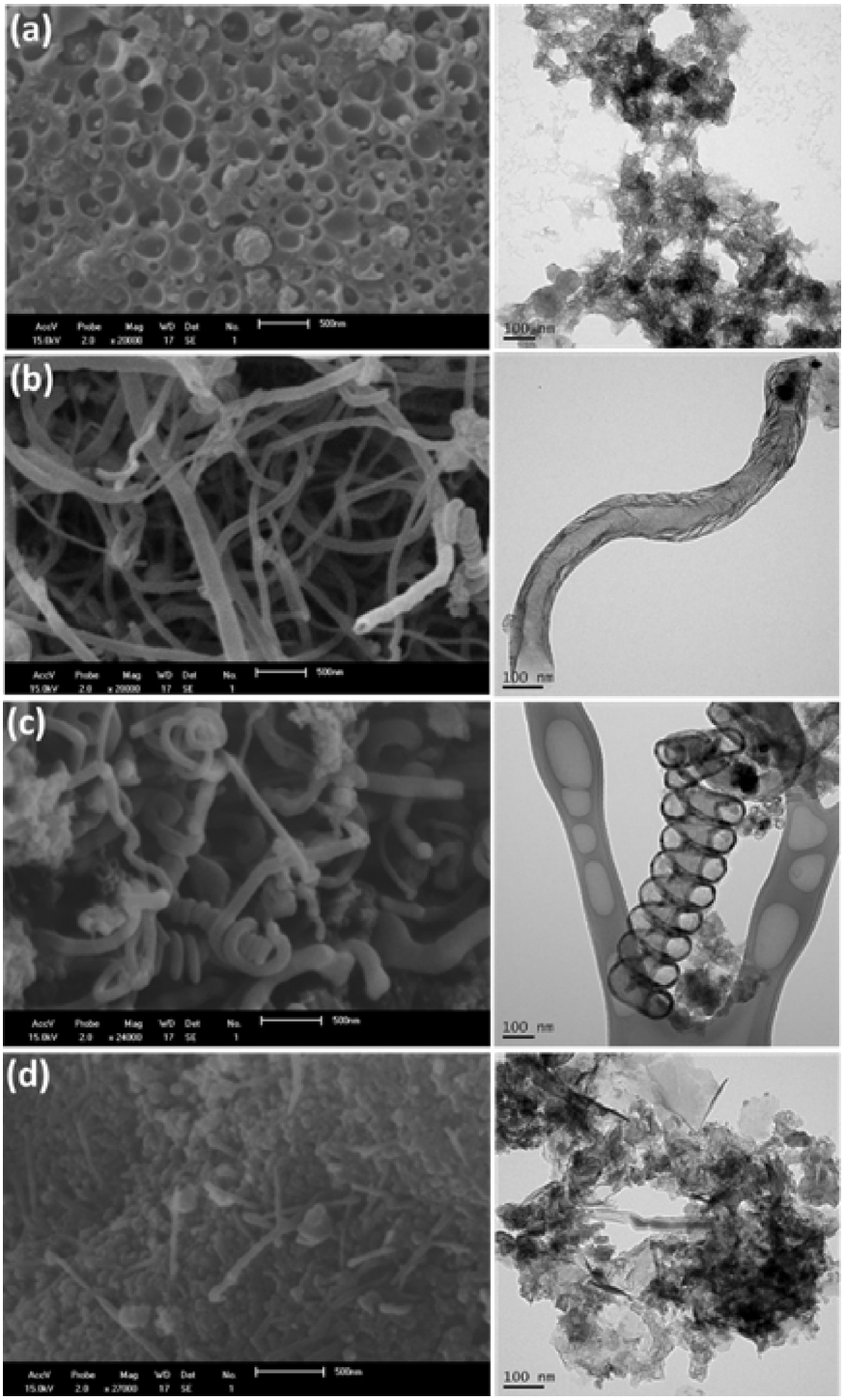

Fig. 2. SEM images (left) and TEM images (right) MFR@Co after pyrolysis at 700 °C (a), 800 °C (b), 900 °C (c), and 1000 °C (d).

ions in the structure closely interact with the intermediates in the organic resin decomposition, and therefore, the final carbonaceous materials obtained is inherently dependent on the metal phase. Thermogravimetric curves of the obtained carbonaceous materials at different pyrolysis temperatures are presented in Fig. 1b. Since TG curves are obtained in air, the onset degradation temperature indicates the chemical stability of the carbonaceous material toward the thermal oxidation, and it is observed that sample prepared at the highest pyrolysis temperate has the highest thermal stability in air, with onset degradation temperature higher than 420 °C. Interestingly, the samples prepared at 800 °C and 900 °C present very similar thermal degradation behavior, around 330 °C.

The residual weight determined by TG curves provides the estimated content of Co in the hybrid material. The values for the different samples are very close among them, varying from 13.4% at 800 °C to 15.9% at 1000 °C. So, there is a predominance of carbonaceous phase over the metal phase in the hybrid materials.

The morphology of the obtained samples can be examined in the SEM and TEM images, Fig. 2. The synthesis parameters have great influence on the morphology of the samples. The shape and homogeneity of the materials obtained after pyrolysis varies according to

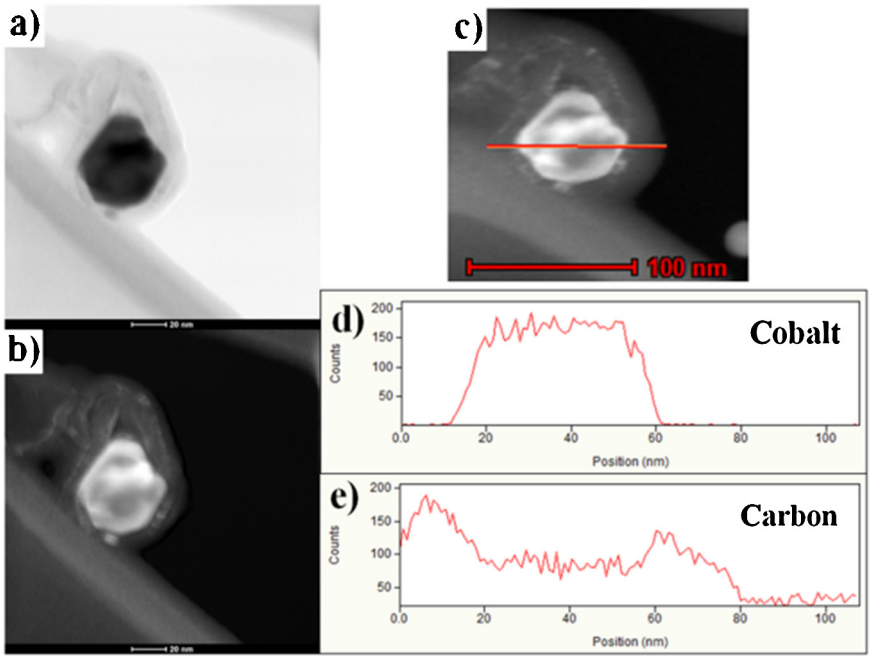

Fig. 3. Bright field TEM image (a), dark field TEM image (b), line profile in dark field image (c), cobalt EDX line scan profile (d), carbon EDX line scan (e).

the pyrolysis temperatures. Dark spherical spots are observed for all the materials. The dark spots are attributed to cobalt phases embodied in the carbon structure. To confirm the identity of these dark spots, high resolution TEM images associated with EDX line analysis were performed. In Fig. 3, bright field and dark field high resolution TEM images of a dark spot, observed in the sample NC@Co-1000, were analyzed. The observed nanoparticle have diameter of c.a. 30 nm. It is possible to confirm the great difference in contrast between the material capping and the nanoparticle. The line analysis indicates the presence of Co signal in the nanoparticle region and show that the counts for cobalt decrease to zero in the region outside of the dark spot, indicating the cobalt presence is restricted to the nanoparticle. The line analysis for carbon indicates that the nanoparticle is surrounded by the carbon matrix.

The temperature dependence on the formation of more organized structures is straightforward observed in the TEM images. The material obtained at lower pyrolysis temperature, 700 °C, does not present a preferential organization with a morphology that is associated to porous amorphous carbon. On the other hand, a great change in the morphology is observed increasing the pyrolysis temperature to 800 °C, in which is observed carbon nanotubes with diameter around 100 nm as the main constituent of the sample. The formed CNT have hollow interior and thick walls. In addition, in the TEM images is also possible to observe the walls of the formed CNT do not present well-organized graphitic alignment. In the CNT are also observed the presence of dark spots attributed to the Co phase, but in this case the particles are occluded in the closed end of the CNT.

Sample prepared at 900 °C is mainly composed of CNTs, but some particles with undefined structures are also observed, SEM image in Fig. 2c. Interestingly, CNTs obtained at 900 °C present some structural differences from those prepared at 800 °C. At higher temperature condition, the nanotubes have more helical shape and the walls are thinner and more compact, indicating a more organized graphitic structure of the concentric layers, which corroborates with Raman spectra. At 900 °C, Co particles also formed inside of the carbon nanotubes.

CNT, observed in the samples produced at 800 °C and 900 °C, are scarcely observed in the sample prepared at 1000 °C (NC@Co-1000). Only few fragments of CNT are identified in the SEM image. NC@Co-1000 is composed of larger structures without preferential shape. Despite of NC@Co-1000 have structures with no preferential shape, the morphology of its structures are not similar to the amorphous framework in the sample NC@Co-700. The effect of the pyrolysis temperature on the carbon matrices is evaluated by the Raman and XRD results, Fig. 4. The Raman spectra of the samples pyrolyzed at different temperatures, Fig. 4a, show similar features, such as the D and G peaks due to hexagonal carbon structure in the regions 1000–1700 cm^{-1}, and a second harmonic peak (i.e. 2D peak) in the region of 2300–3300 cm^{-1} [39]. I_D/I_G ratio is used here to evaluate the organization of the carbon material obtained at each pyrolysis temperature [40]. As expected, I_D/I_G reduces according to the increase of the temperature, and therefore the degree of organization of the carbon structure increases constantly. It is worth noting that the particle shape is not directly correlated to the organization measured by Raman. For instance, the sample prepared at 1000 °C, which does not have any preferential particle shape, has a higher organization level than the helical nanotubes obtained at 900 °C.

The Raman spectra also allow the verification of peaks in the range of 400 to 750 cm^{-1}, attributed to the presence of Co_3O_4 crystalline phase [41]. Co_3O_4 crystalline phase have four characteristic peaks located at 464, 507, 606, and 675 cm^{-1} attributed to E_g, $F_{2g}{}^1$, $F_{2g}{}^2$, and $A_g{}^1$ modes, where the peak at 675 cm^{-1} is the most intense [42]. For all samples but the one prepared at 700 °C, it is possible to observe a peak of very low intensity at 675 cm^{-1} revealing the presence of the phase Co_3O_4, Figure S1. Taking the intensity of the 675 cm^{-1} as reference, it can be said that the sample with higher content of Co_3O_4 phase is the sample prepared at highest pyrolysis temperature. The increase in observed amount of Co_3O_4 as per the temperature increase will be further discussed in this manuscript, correlating the Raman data with XPS results.

The XRD results, Fig. 4b, are in complete agreement with the results found by Raman in respect to the graphitization level of the carbonaceous matrices. First, the amorphous halo attributed to the amorphous carbon centered at 26°, found for sample prepared at 700 °C and 800 °C, is replaced by a narrower peak placed at 27° attributed to the graphitic crystalline phase, for the samples

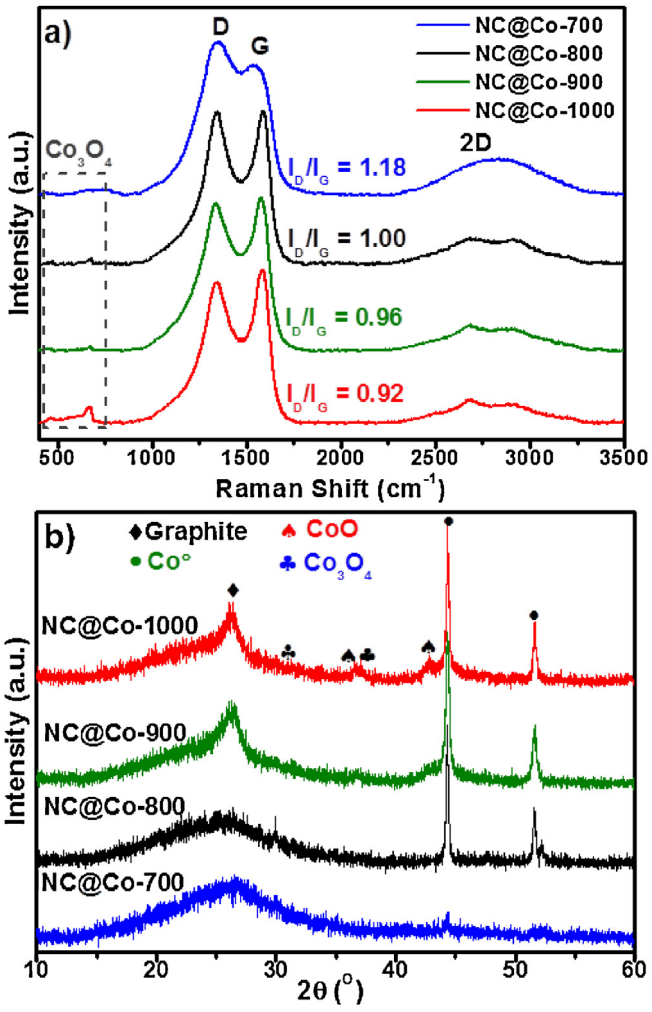

Fig. 4. Raman spectra (a) and XRD diffractograms (b) of the sample pyrolyzed at different temperatures.

prepared at 900 °C and 1000 °C. The presence of the graphitic peak indicates the formation of well-organized multi walls arrangement in the helical nanotubes at 900 °C, while the nanotubes formed at 800 °C have more disorganized wall structure. In addition, even though the sample prepared at 1000 °C does not have preferential particle shape, it possesses the highest degree of graphitization as observed in both Raman and XRD.

Further information about the structural characteristics of the samples is provided by the N_2 adsorption/desorption experiments, Figure S2. The isotherms can be classified as type IV, which is due to the presence of mesopores, since at higher pressures the slopes show increased uptake of N_2 as pores become filled. It is also observed hysteresis between adsorption and desorption branches of the isotherms, which is an indication of the capillary effect of the mesopores. Sample synthesized at 700 °C presents a H4 hysteresis type, what is normally found for micro and mesoporous carbon [43], while all other samples are classified with H2 hysteresis type, what is attributed to more complex structures as a consequence of the interconnectivity of pores [44].

The chemical composition of the hybrid materials surface is revealed by XPS. The XPS survey and high resolution spectra are presented in the Figures S3 to S6, in the supporting information. The elemental composition obtained from the survey is presented in the Table S1. In Fig. 5a is presented the nitrogen content as function of the pyrolysis temperature, which goes through a severe reduction with the temperature increase. The sample prepared at

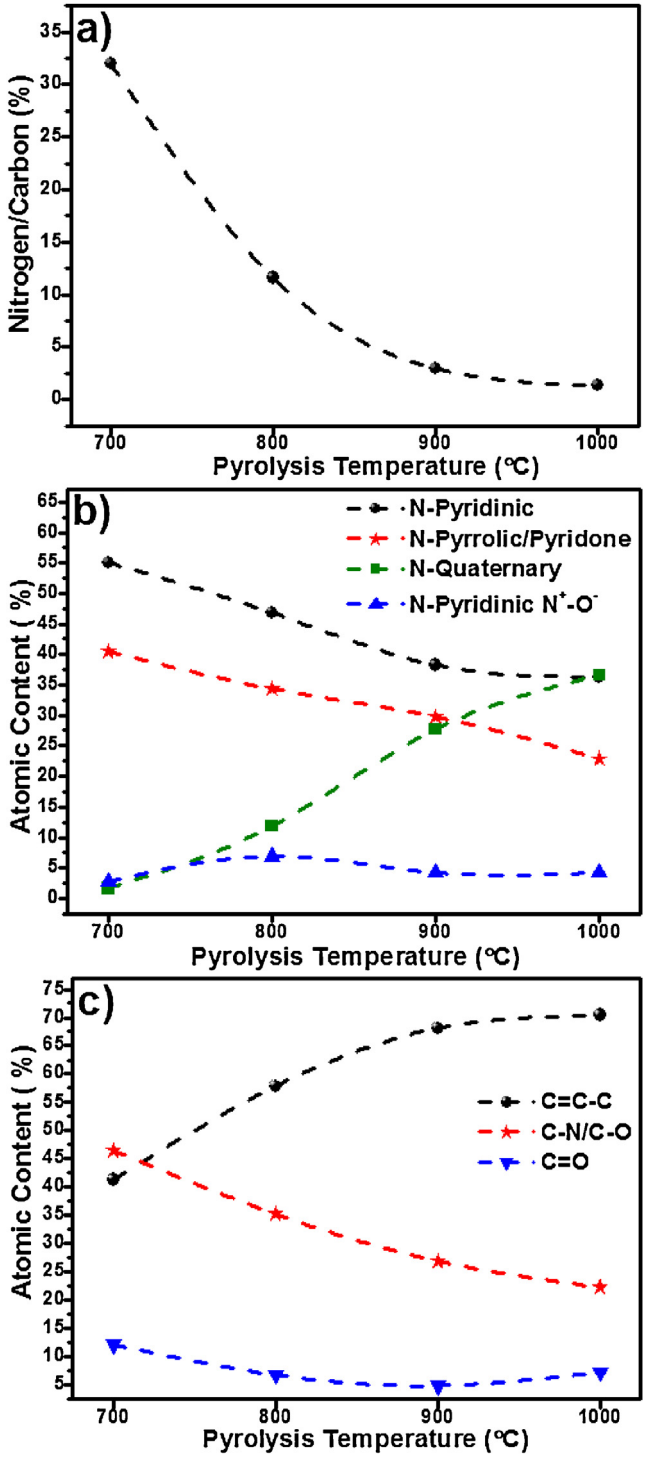

Fig. 5. XPS chemical composition data in function of the pyrolysis temperature. (a) nitrogen/carbon ratio content, (b) relative content of nitrogen containing groups, and (c) relative content of peaks attribution to carbon signal.

700 °C presents 31.97% of N/C ratio, indicating the ability of the MFR to produce a carbonaceous material with elevated N content. The decrease in the nitrogen content is expected as the temperature increases following literature result [18,45]. However, in the case of the MRF with Co^{2+} coordinated the reduction is almost exponential. The increase of pyrolysis temperature to 800 °C causes a reduction of the N/C ratio to 11.62%. The drastic change in the nitrogen content can be correlated to the morphological change that occur in this range, once the sample with 31.97% of N/C is amor-

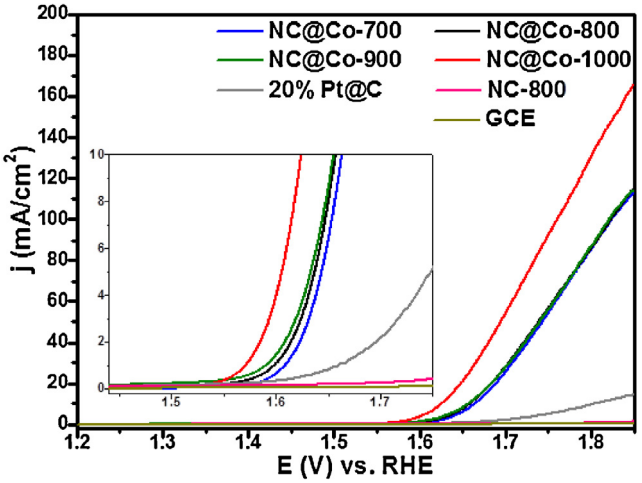

Fig. 6. Polarization curves measured in a RDE electrode at 1000 rpm using glassy carbon as working electrode modified with synthesized hybrid materials in a 1.0 M KOH solution saturated with N_2 and scan rate of 20 mV s^{-1}.

phous material and the sample with 11.62% is formed by carbon nanotubes. The organization process of the carbonaceous materials is favored by the nitrogen elimination during the pyrolysis. This correlation is even more evidenced by the increase of the temperature to 900 °C that leads to helical carbon nanotubes, in which the N/C ratio drop to 2.95%. The graphitic porous structure obtained at 1000 °C has only 1.35% of N/C and the highest degree of organization as demonstrated by Raman and XRD.

The elemental composition of the samples, determined by XPS, also demonstrates an interesting behavior for the cobalt content at the surface. The cobalt content increases with the pyrolysis temperature. In the sample NC@Co-700 it was found that Co content at the surface is 1.69%. The Co content increase to the maximum value observed of 6.08% found for the sample CN@Co-1000. This result can be used to explain the increase of the Raman peaks attributed to Co oxides phases in function of the temperature. At higher temperatures, the Co particles are more exposed to the surface and as consequence a more prominent amount of Co_3O_4 phase is formed. Therefore, at higher temperatures the Co particles have higher tendency to migrate to the surface of the carbon matrices. Such behavior was previous observed by Silva et al. that evaluated the formation and the migration of Ag nanoparticles in polymer matrices [46]. Metal particles are more easily expelled from the continuous phase at higher temperature due to higher mobility of the matrix components.

The decrease of the overall content of nitrogen have also affect the relative content of nitrogen containing groups, Fig. 5b. At 700 °C the sample is mainly constituted of pyridinic and pyrrolic nitrogen, and the content of these two groups decreases linearly with the pyrolysis temperature increase. On the other hand, quaternary group is almost absent in the sample prepared at 700 °C and it increases to become the most abundant nitrogen containing group at 1000 °C. The decrease of heteroatoms content in the hybrid material is also demonstrated by the carbon signal, Fig. 5c, where the contribution of C-N/C-O signal to the total carbon peak decrease from 46% to 22%, from 700 °C to 1000 °C, respectively.

The hybrid material containing the metallic cobalt enclosed is applied as catalyst for the oxygen evolution reaction in strong basic condition. The polarization curves for the samples are presented in Fig. 6 and reveal a strong activity of the modified working electrode in comparison to bare GCE and also a blank sample prepared without the presence of Co. Among the samples, the prepared at 1000 °C stands out with an overpotential at least 40 mV better than any sample prepared at a different temperature. In fact, it can be observed a general trend indicating that an increasing at the pyrolysis temperature improves the catalytic activity. However, the improvement in the catalytic activity from 700 °C to 900 °C is modest, but it is accentuated from 900 °C to 1000 °C. In the XRD results, we observed that all the samples have Co° as the main cobalt phase. Only in the case of the sample prepared at 1000 °C it is possible to observe a weaker diffraction peaks indicating the presence of CoO and Co_3O_4 phases as minor components. The oxides phase is more likely to be present as passivated layers of the Co NPs. Therefore, the catalytic activity found has to be mainly attributed to Co^0 phase. Indeed, it can be evidenced by normalizing the current by Co mass loaded on GCE, Figure S7, which demonstrate the same general trend toward OER activity as aforementioned. On the other hand, the presence of small relative amounts of CoO and Co_3O_4 in the sample prepared at 1000 °C is a possible explanation for its higher activity.

The electrochemically active area of Co is a difficult parameter to measure since the Co nanoparticles are embedded in carbon structures. For instance, capacitance experiments cannot be related to the electrochemically active surface area (ECSA) for hybrid metal-carbon materials since the capacitance of the samples mainly derives from carbon [47]. Then, a new approach was used to calculate the electrochemically active surface area derived merely from Co. After the catalyst casting on the working electrode, the electrode was placed in a 10 mM $Cu(NO_3)_2$ solution for 20 min in order to replace the metallic Co on carbon's surface by metallic Cu. It occurs due to galvanic replacement process of Co by Cu, a spontaneous redox reaction. Afterwards the metallic Cu, spontaneously formed on the electrode, was electrochemically stripped in 0.5 M H2SO4 solution (Figure S8a). The charges involved in the voltammetric measurements were converted to ECSA by the following equation [48]:

$$\mathrm{ECSA} = Q_{Cu}/Q_{Cu,M}$$

where Q_{Cu} is the charge transferred in Cu stripping process and $Q_{Cu,M}$ is the charge corresponding to deposited Cu monolayer per unity area. The $Q_{Cu,M}$ value used was 410 μC/cm² [48]. Figure S8b presents the correlation between the η@10 mA cm^{-2} and the ECSA as function of pyrolysis temperature, where is clearly observed a decrease of the η@10 mA/cm² as ECSA increases. The results, provided by normalizing the current by Co-ECSA (Figure S8c), are in agreement with the discussion aforementioned, the sample pyrolyzed at the highest temperature has the best catalytic activity toward OER due the highest amount of available Co at the catalyst surface.

An important information to justify the increase of the catalytic activity with the increase of the temperature can be observed in the XPS results, Table S1. The cobalt content in the sample analyzed by XPS increase from 1.69% to 6.08%, from 700 °C to 1000 °C. XPS is a surface analysis and therefore, it can be understood that the increase of the pyrolysis temperate increase the Co exposition. Therefore, the cobalt is more likely to participate of the OER reaction in the sample prepared at 1000 °C.

The use of the metallic cobalt as catalytic agent for OER has some relevant precedents in the literature. Wu et al. used a system composed of deposited arrays of Co NPs from the thermal decomposition of a $[Co_2(CO)_8]$, that leads to Co particles capped by carbon from the CO decomposition on metallic Co, to carry the OER process with 390 mV (no *iR*-correction) of overpotential in the best case [49]. In addition, Jin et al. reported a hybrid material composed of Co^0, CoO, and Co_3O_4 embedded in amorphous N-doped carbon from melamine and *D*(+)-glucosamine hydrochloride [47]. The results indicate the most active Co phase is CoO, which could perform OER at 232 mV (*iR*-corrected) at 10 mA cm^{-2} of overpotential using Ni foam loaded with 2.1 mg cm^{-2}.

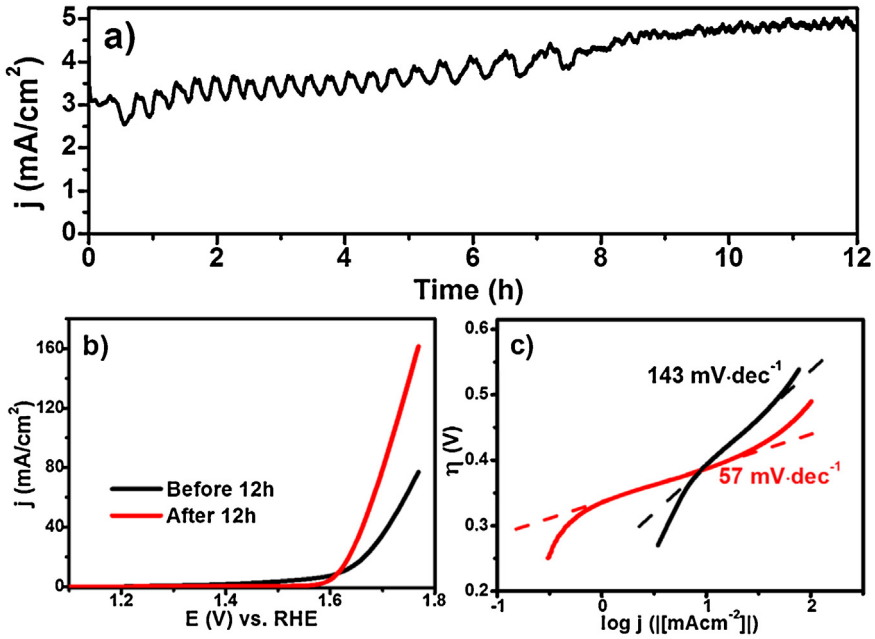

Fig. 7. Chronoamperometry analysis of the sample prepared at 1000 °C applying an over potential of 360 mV using an electrolyte solution of 1.0 M KOH(a), LSV of the sample before and after the chronoamperometry analysis(b), and Tafel plot (c).

Interestingly, a blank sample prepared only by the pyrolysis of the carbon precursor material does not present catalytic activity toward OER. The direct effect of the nitrogen doped carbon on the OER is, therefore, excluded. The lack of activity of nitrogen species on the carbon over OER is also demonstrated by the opposite trend between N content among and catalytic activity. Increasing temperature of pyrolysis, the nitrogen content drops down and the catalytic activity increases.

The stability of the hybrid material, prepared at 1000 °C, toward the OER demonstrates a remarkable pattern. The sample was analyzed by chronoamperometry, Fig. 7, for 12 h of constant applied potential. The chronoamperometric curve is noisy due the formation of O_2 bubbles that sticks and after reach a determined size detaches from the work electrode. It is observed that the current density increase consistently over time in the first 8 h of use in a self-activation process. After 12 h of direct use it is observed a value of *j* 52% higher than the initial value. It means that the catalyst is strongly activated during the electrochemical process and after it reaches the best catalytic activity it will degrade and then loss its activity. Interestingly, Co^0 enclosed in carbon matrix was reported before but the self-activation process was not observed [49]. Therefore, porous graphitic carbon matrix plays an important role in this process because the pores allows the diffusion of the electrolyte solution and the organized graphitic structure acts to protect the Co to be leached out by the oxidation process. After the current density stabilizes, around 8 h of use, the curve is very stable. Therefore, the results indicate the catalyst has an exceptional stability, without any precedent in the literature. For instance, Co^0 enclosed in carbon from the decomposition of $[Co_2(CO)_8]$ lost more than 50% of its activity after 6 h of use [49]. The deactivation of the catalyst is normally correlated to the carbon matrix failure leading to the decrease of conductivity or to the metal leaching. In addition, the cobalt oxidation should occur but it is limited by the tight confinement provided by the carbon matrix. Depending on the structured of the carbon matrix the hosted species can be kept protected from oxidation even in harsh environment [50]. In order to investigate the OER activity improvement was performed Raman spectra of the NC@Co-1000 supported in FTO-glass as prepared and after the chronoamperometric measurement, Figure S9. After the 12 h of constant applied potential, the oxide peaks in 675 cm^{-1} and 194 cm^{-1} undergoes a downshift of ca. 10 cm^{-1} to 664 cm^{-1} and 184 cm^{-1}, Figure S8a, while the carbon peaks show no shift. The peaks in 664 cm^{-1} and 184 cm^{-1} are attributed to CoO phase [51] that might be formed due the oxidation of the metallic Co during the OER process. As aforementioned, Wang et al. [47] indicate that the most Co active phase toward OER is the CoO phase, thus an increasing of CoO amount during the oxygen evolution can be a possible reason for the OER activity improvement over the time.

Changes in the materials active in function of the use was analyzed by LSV. LSV curves of an electrode, before and after 12 h of applied potential, is shown in Fig. 7b. It is observed that both onset potential and the slope of the current density are improved after 12 h of use for OER. However, the difference seems to be mainly associated with the shape of the curve that indicates a reduction of the electron transfers resistance. The Tafel slope undergoes a severe change after the 12 h of OER. The Tafel slope value that initially was of 61 mV dec^{-1} is characteristic of the predominance of surface adsorbed species produced in the early stage of the OER. The Tafel slope has initially a very large value of 143 mV dec^{-1}, which can be related to a sluggish kinetics of electron transference. After 12 h the Tafel slope reduce to 57 mV dec^{-1}, that is characteristic of the predominance of surface adsorbed species produced in the early stage of the OER [52]. Such small values (~60 mV dec^{-1}) were previously reported for NiCo layered double hydroxide [53] and, for the state-of-the-art, Ir/C [54]. This Tafel slope value demonstrates the unique features of the Co particles tightly embodied in the graphitic carbon.

4. Conclusions

MFR is proposed as a possible precursor to hybrid material by the coordination of Co^{2+} ions in the starting precursor. The presented method can be used to produce different materials with the aid of pyrolysis temperature. The system allows the obtaining of nitrogen doped carbon, with more than 30% of nitrogen, and amorphous structure. Carbon nanotubes can also be resulted from the synthesis of appropriated temperature range. The structure of the obtained carbon nanotubes can be tuned by the temperature. It

was observed nanotubes with more than 11% of nitrogen and not well graphitized walls at 800 °C, while carbon nanotubes obtained at 900 °C have preferential helical structure and much lower nitrogen content, around 3% of nitrogen. Besides amorphous carbon and carbon nanotubes, a distinct porous graphitic carbon is verified at the highest tested temperature with the lowest nitrogen content of 1.35%.

In the precursor material is added Co^{2+}, which is converted to metallic Co^0 phase in the hybrid material. It is expected Co^0 NPs to get easily oxidized in environmental condition due the low stability of Co NPs. In the present case, the Co^0 is stable over time, indication a strong passivation effect of the carbon matrix. However, in the case of the sample prepared at 1000 °C is proved by Raman and XRD the present of CoO and Co_3O_4 phase, but at very low level due the weak signals in the XRD diffractogram.

The most active material proved to be the porous graphitic carbon, which have the lower nitrogen content, but vestiges of CoO and Co_3O_4 phases. However, all other material showed to be nearly active, and they could be considered as efficient catalysts due to the overpotential at 10 mA cm^{-2} to be in the range from 390 to 450 mV.

A very important aspect found is the remarkable stability of the synthesized catalyst that has its activity improved in the first 8 h of use and then a very stable behavior. This effect is not observed to akin materials reported in the literature and organized carbon structure in the sample prepared from the MFR is believed to be the major factor to hinder the deactivations phenomena.

Acknowledgements

GMP thanks the Coordenação de Aperfeiçoamento de Pessoal de Nível Superior (CAPES-Brasil) for doctorate fellowships. AFR and RS acknowledges the financial supports given by CNPq, Coordenação de Aperfeiçoamento de Pessoal de Nível Superior (CAPES-Brasil) and Fundação Araucária-Brasil.

Appendix A. Supplementary data

Supplementary data associated with this article can be found, in the online version, at 10.1016/j.apcatb.2017.05.056.

References

[1] D. Jariwala, V.K. Sangwan, L.J. Lauhon, T.J. Marks, M.C. Hersam, Carbon nanomaterials for electronics, optoelectronics, photovoltaics, and sensing, Chem. Soc Rev. 42 (2013) 2824–2860.
[2] W. Yang, K.R. Ratinac, S.P. Ringer, P. Thordarson, J.J. Gooding, F. Braet, Carbon nanomaterials in biosensors: should you use nanotubes or graphene? Angew. Chem.-Int. Ed. 49 (2010) 2114–2138.
[3] M.S. Mauter, M. Elimelech, Environmental applications of carbon-based nanomaterials, Environ. Sci. Technol. 42 (2008) 5843–5859.
[4] B. Smith, K. Wepasnick, K.E. Schrote, H.-H. Cho, W.P. Ball, D.H. Fairbrother, Influence of surface oxides on the colloidal stability of multi-walled carbon nanotubes: a structure-property relationship, Langmuir 25 (2009) 9767–9776.
[5] E. Frackowiak, F. Beguin, Carbon materials for the electrochemical storage of energy in capacitors, Carbon 39 (2001) 937–950.
[6] J.-P. Tessonnier, D. Rosenthal, T.W. Hansen, C. Hess, M.E. Schuster, R. Blume, F. Girgsdies, N. Pfaender, O. Timpe, D.S. Su, R. Schloegl, Analysis of the structure and chemical properties of some commercial carbon nanostructures, Carbon 47 (2009) 1779–1798.
[7] C. Dominguez, F.J. Perez-Alonso, M.A. Salam, S.A. Al-Thabaiti, M.A. Pena, F.J. Garcia-Garcia, L. Barrio, S. Rojas, Repercussion of the carbon matrix for the activity and stability of Fe/N/C electrocatalysts for the oxygen reduction reaction, Appl. Catal. B-Environ. 183 (2016) 185–196.
[8] R. Silva, J. Al-Sharab, T. Asefa, Edge-plane-rich nitrogen-doped carbon nanoneedles and efficient metal-free electrocatalysts, Angew. Chem.-Int. Ed. 51 (2012) 7171–7175.
[9] M.I. Katsnelson, Graphene: carbon in two dimensions, Mater. Today 10 (2007) 20–27.
[10] N.A. Kaskhedikar, J. Maier, Lithium storage ion carbon nanostructures, Adv. Mater. 21 (2009) 2664–2680.
[11] J. Yu, G. Chen, J. Sunarso, Y. Zhu, R. Ran, Z. Zhu, W. Zhou, Z. Shao, Cobalt oxide and cobalt-graphitic carbon core–shell based catalysts with remarkably high oxygen reduction reaction activity, Adv. Sci. 3 (2016), 1600060-n/a.
[12] V.C. Almeida, R. Silva, M. Acerce, O. Pezoti Junior, A.L. Cazetta, A.C. Martins, X. Huang, M. Chhowalla, T. Asefa, N-doped ordered mesoporous carbons with improved charge storage capacity by tailoring N-dopant density with solvent-assisted synthesis, J. Mater. Chem. A 2 (2014) 15181–15190.
[13] R. Silva, G.M. Pereira, D. Voiry, M. Chhowalla, T. Asefa, Co_3O_4 nanoparticles/cellulose nanowhiskers-derived amorphous carbon nanoneedles: sustainable materials for supercapacitors and oxygen reduction electrocatalysis, RSC Adv. 5 (2015) 49385–49391.
[14] J.P. Paraknowitsch, A. Thomas, Doping carbons beyond nitrogen: an overview of advanced heteroatom doped carbons with boron, sulphur and phosphorus for energy applications, Energy Environ. Sci. 6 (2013) 2839–2855.
[15] E. Bayram, G. Yilmaz, S. Mukerjee, A solution-based procedure for synthesis of nitrogen doped graphene as an efficient electrocatalyst for oxygen reduction reactions in acidic and alkaline electrolytes, Appl. Catal. B-Environ. 192 (2016) 26–34.
[16] Z.X. Fan, X. Huang, C.L. Tan, H. Zhang, Thin metal nanostructures: synthesis, properties and applications, Chem. Sci. 6 (2015) 95–111.
[17] G. Wu, P. Zelenay, Nanostructured nonprecious metal catalysts for oxygen reduction reaction, Acc. Chem. Res. 46 (2013) 1878–1889.
[18] R. Silva, D. Voiry, M. Chhowalla, T. Asefa, Efficient metal-free electrocatalysts for oxygen reduction: polyaniline-derived n- and o-doped mesoporous carbons, J. Am. Chem. Soc. 135 (2013) 7823–7826.
[19] R.A. Araujo, A.F. Rubira, T. Asefa, R. Silva, Metal doped carbon nanoneedles and effect of carbon organization with activity for hydrogen evolution reaction (HER), Carbohydrate Polym. 137 (2016) 719–725.
[20] P. Iamprasertkun, A. Krittayavathananon, M. Sawangphruk, N-doped reduced graphene oxide aerogel coated on carboxyl-modified carbon fiber paper for high-performance ionic-liquid supercapacitors, Carbon 102 (2016) 455–461.
[21] B. You, F. Kang, P. Yin, Q. Zhang, Hydrogel-derived heteroatom-doped porous carbon networks for supercapacitor and electrocatalytic oxygen reduction, Carbon 103 (2016) 9–15.
[22] L. Qie, W. Chen, H. Xu, X. Xiong, Y. Jiang, F. Zou, X. Hu, Y. Xin, Z. Zhang, Y. Huang, Synthesis of functionalized 3D hierarchical porous carbon for high-performance supercapacitors, Energy Environ. Sci. 6 (2013) 2497–2504.
[23] X. Wang, X. Li, L. Zhang, Y. Yoon, P.K. Weber, H. Wang, J. Guo, H. Dai, N-doping of graphene through electrothermal reactions with ammonia, Science 324 (2009) 768–771.
[24] L.S. Panchokarla, K.S. Subrahmanyam, S.K. Saha, A. Govindaraj, H.R. Krishnamurthy, U.V. Waghmare, C.N.R. Rao, Synthesis, structure, and properties of boron- and nitrogen-doped graphene, Adv. Mater. 21 (2009), 4726-+.
[25] X. Li, J. Shi, T. Zhao, R. Wan, C. Leng, Y. Lei, Structural and electronic properties study on B-N co-doped (4,3) carbon nanotubes through first-principles calculations, Physica B-Condens. Matter 490 (2016) 63–72.
[26] S. Yasuda, A. Furuya, Y. Uchibori, J. Kim, K. Murakoshi, Iron-nitrogen-doped vertically aligned carbon nanotube electrocatalyst for the oxygen reduction reaction, Adv. Funct. Mater. 26 (2016) 738–744.
[27] L. Yang, Y. Xia, X. Fan, L. Qin, B. Qiu, Z. Liu, Constructing durable carbon layer on LiMn0.8Fe0.2PO4 with superior long-term cycling performance for lithium-ion battery, Electrochim. Acta 191 (2016) 200–206.
[28] R. Tang, Q. Yun, W. Lv, Y.-B. He, C. You, F. Su, L. Ke, B. Li, F. Kang, Q.-H. Yang, How a very trace amount of graphene additive works for constructing an efficient conductive network in $LiCoO_2$-based lithium-ion batteries, Carbon 103 (2016) 356–362.
[29] Y.-L. Ding, P. Kopold, K. Hahn, P.A. van Aken, J. Maier, Y. Yu, Facile solid-state growth of 3D well-interconnected nitrogen-rich carbon nanotube-graphene hybrid architectures for lithium-sulfur batteries, Adv. Funct. Mater. 26 (2016) 1112–1119.
[30] X.X. Zou, X.X. Huang, A. Goswami, R. Silva, B.R. Sathe, E. Mikmekova, T. Asefa, Cobalt-embedded nitrogen-rich carbon nanotubes efficiently catalyze hydrogen evolution reaction at all pH Values**, Angew. Chem.-Int. Ed. 53 (2014) 4372–4376.
[31] O. Krocher, M. Elsener, Materials for thermohydrolysis of urea in a fluidized bed, Chem. Eng. J. 152 (2009) 167–176.
[32] M. Tavakkoli, T. Kallio, O. Reynaud, A.G. Nasibulin, C. Johans, J. Sainio, H. Jiang, E.I. Kauppinen, K. Laasonen, Single-shell carbon-encapsulated iron nanoparticles: synthesis and high electrocatalytic activity for hydrogen evolution reaction, Angew. Chem.-Int. Ed. 54 (2015) 4535–4538.
[33] M.W. Kanan, D.G. Nocera, In situ formation of an oxygen-evolving catalyst in neutral water containing phosphate and Co2+, Science 321 (2008) 1072–1075.
[34] V. Artero, M. Chavarot-Kerlidou, M. Fontecave, Splitting water with cobalt, Angew. Chem.-Int. Ed. 50 (2011) 7238–7266.
[35] X.H. Deng, H. Tuysuz, Cobalt-oxide-based materials as water oxidation catalyst: recent progress and challenges, ACS Catal. 4 (2014) 3701–3714.
[36] C. Nam Hawn, P.N. Ross, A.T. Bell, T.D. Tilley, Comparison of cobalt-based nanoparticles as electrocatalysts for water oxidation, ChemSusChem 4 (2011) 1566–1569.
[37] I.H. Anderson, M. Cawley, W. Steedman, Melamine - formaldehyde resins II. -Thermal degradation of model compounds and resins, Br. Polym. J. 3 (1971).
[38] V.C. Almeida, R. Silva, M. Acerce, O. Pezoti, A.L. Cazetta, A.C. Martins, X.X. Huang, M. Chhowalla, T. Asefa, N-doped ordered mesoporous carbons with improved charge storage capacity by tailoring N-dopant density with solvent-assisted synthesis, J. Mater. Chem. A 2 (2014) 15181–15190.

[39] A.C. Ferrari, D.M. Basko, Raman spectroscopy as a versatile tool for studying the properties of graphene, Nat. Nanotechnol. 8 (2013) 235–246.
[40] A. Pendashteh, J. Palma, M. Anderson, R. Marcilla, NiCoMnO4 nanoparticles on N-doped graphene: Highly efficient bifunctional electrocatalyst for oxygen reduction/evolution reactions, Appl. Catal. B-Environ. 201 (2017) 241–252.
[41] J. Gonzalez-Prior, R. Lopez-Fonseca, J.I. Gutierrez-Ortiz, B. de Rivas, Oxidation of 1,2-dichloroethane over nanocube-shaped Co3O4 catalysts, Appl. Catal. B-Environ. 199 (2016) 384–393.
[42] J. Zhang, W.B. Gao, M.L. Dou, F. Wang, J.J. Liu, Z.L. Li, J. Ji, Nanorod-constructed porous Co3O4 nanowires: highly sensitive sensors for the detection of hydrazine, Analyst 140 (2015) 1686–1692.
[43] M.Y. Song, D.S. Yang, K.P. Singh, J.L. Yuan, J.S. Yu, Nitrogen-doped hollow carbon spheres with highly graphitized mesoporous shell: Role of Fe for oxygen evolution reaction, Appl. Catal. B-Environ. 191 (2016) 202–208.
[44] K.S.W. Sing, D.H. Everett, R.A.W. Haul, L. Moscou, R.A. Pierotti, J. Rouquerol, T. Siemieniewska, Reporting physisorption data for gas solid systems with special reference to the determination of surface-area and porosity (recommendations 1984), Pure Appl. Chem. 57 (1985) 603–619.
[45] M. Li, J.M. Xue, Integrated synthesis of nitrogen-doped mesoporous carbon from melamine resins with superior performance in supercapacitors, J. Phys. Chem. C 118 (2014) 2507–2517.
[46] R. Silva, M.H. Kunita, E.M. Girotto, E. Radovanovic, E.C. Muniz, G.M. Carvalho, A.F. Rubira, Synthesis of Ag-PVA and Ag-PVA/PET-s20 composites by supercritical CO_2 method and study of silver nanoparticle growth, J. Braz. Chem. Soc. 19 (2008) 1224–1229.
[47] H. Jin, J. Wang, D. Su, Z. Wei, Z. Pang, Y. Wang, In situ cobalt–cobalt oxide/N-doped carbon hybrids as superior bifunctional electrocatalysts for hydrogen and oxygen evolution, J. Am. Chem. Soc. 137 (2015) 2688–2694.
[48] M. Lukaszewski, M. Soszko, A. Czerwinski, Electrochemical methods of real surface area determination of noble metal electrodes - an overview, Int. J. Electrochem. Sci. 11 (2016) 4442–4469.
[49] L. Wu, Q. Li, C.H. Wu, H. Zhu, A. Mendoza-Garcia, B. Shen, J. Guo, S. Sun, Stable cobalt nanoparticles and their monolayer array as an efficient electrocatalyst for oxygen evolution reaction, J. Am. Chem. Soc. 137 (2015) 7071–7074.
[50] J. Tuček, Z. Sofer, D. Bouša, M. Pumera, K. Holá, A. Malá, K. Poláková, M. Havrdová, K. Čépe, O. Tomanec, R. Zbořil, Air-stable superparamagnetic metal nanoparticles entrapped in graphene oxide matrix, Nat. Commun. 7 (2016) 12879.
[51] X.M. He, X.Y. Song, W. Qiao, Z.W. Li, X. Zhang, S.M. Yan, W. Zhong, Y.W. Du, Phase- and size-dependent optical and magnetic properties of CoO nanoparticles, J. Phys. Chem. C 119 (2015) 9550–9559.
[52] T. Shinagawa, A.T. Garcia-Esparza, K. Takanabe, Insight on Tafel slopes from a microkinetic analysis of aqueous electrocatalysis for energy conversion, Sci. Rep. 5 (2015) 13801.
[53] F. Song, X.L. Hu, Exfoliation of layered double hydroxides for enhanced oxygen evolution catalysis, Nat. Commun. 5 (2014).
[54] Z. Lu, W.W. Xu, W. Zhu, Q. Yang, X.D. Lei, J.F. Liu, Y.P. Li, X.M. Sun, X. Duan, Three-dimensional NiFe layered double hydroxide film for high-efficiency oxygen evolution reaction, Chem. Commun. 50 (2014) 6479–6482.